Transport coefficients of the Lennard-Jones model fluid. I. Viscosity

Karsten Meier[a)]
Institut für Thermodynamik, Helmut-Schmidt-Universität–Universität der Bundeswehr Hamburg, Holstenhofweg 85, D-22043 Hamburg, Germany

Arno Laesecke
Physical and Chemical Properties Division, Chemical Science and Technology Laboratory, National Institute of Standards and Technology, Boulder, Colorado 80305

Stephan Kabelac
Institut für Thermodynamik, Helmut-Schmidt-Universität–Universität der Bundeswehr Hamburg, Holstenhofweg 85, D-22043 Hamburg, Germany

(Received 3 February 2004; accepted 17 May 2004)

In an extensive computer simulation study, the transport coefficients of the Lennard-Jones model fluid were determined with high accuracy from equilibrium molecular-dynamics simulations. In the frame of time-correlation function theory, the generalized Einstein relations were employed to evaluate the transport coefficients. This first of a series of four papers presents the results for the viscosity, and discusses and interprets the behavior of this transport coefficient in the fluid region of the phase diagram. Moreover, the kinetic-kinetic, kinetic-potential, and potential-potential viscosity contributions are resolved over the whole range of fluid states, and their characteristic dependence on temperature and density is described. Finally, an additional analysis of the shear-stress correlation functions reveals aspects of the momentum-transport mechanisms on the molecular scale. © *2004 American Institute of Physics.* [DOI: 10.1063/1.1770695]

I. INTRODUCTION

This work aims at the computation of the transport coefficients of the Lennard-Jones potential in the fluid region of the phase diagram by equilibrium molecular-dynamics simulations using time-correlation function theory.

In general, several theoretical approaches are available to calculate transport coefficients from a knowledge of the intermolecular forces. For example, kinetic theory as described by the Boltzmann equation has been successfully applied to calculate transport coefficients for dilute gases in the limit of zero density.[1] On the other hand, time-correlation function theory can be applied at arbitrary densities and temperatures. In this theory, transport coefficients are either expressed as integrals of time-correlation functions of their corresponding thermodynamic fluxes or they are related to the slope of generalized mean-squared displacement functions, which are proportional to the center of the transported quantity in the system.[2] These approaches are the well-known Green-Kubo integrals and Einstein relations. Among others, McLennan and Swenson[3] proved that in the zero-density limit time-correlation function theory yields the same results for the transport coefficients of monatomic fluids as the Chapman-Enskog solution to the Boltzmann equation.[1] These proofs employed the Boltzmann equation or some generalized kinetic equation to evaluate the Green-Kubo formulas. A calculation of the zero-density viscosity and thermal conductivity based entirely on time-correlation function theory was recently carried out by Alavi and Snider.[4] In subsequent papers, Snider and Alavi[5] derived expressions for the second viscosity and thermal-conductivity virial coefficients for purely repulsive intermolecular potentials from time-correlation function theory and showed that their results agree with those obtained by Curtiss and co-workers[6] from a generalized Boltzmann equation by means of kinetic theory. Except for the zero-density transport coefficients and the second transport virial coefficients, accurate solutions to the Green-Kubo integral formulas have not yet been obtained due to the complexity of the transport mechanisms on the molecular scale. Transport coefficients at arbitrary fluid states can at present be computed only by means of molecular-dynamics simulations.

Idealized intermolecular potential models, such as the hard sphere, square well, or Lennard-Jones potentials, are often employed to predict transport coefficients of real fluids or to study transport mechanisms on the molecular scale. In applications of statistical thermodynamics, they serve as simple models for fluids consisting of spherical molecules or, for instance in the united atom approach,[7] as a building block for structural groups in complex molecules such as long-chain alkanes, polymers, or even proteins. Furthermore, precise simulation data for transport coefficients of these model fluids serve as references for testing new theories or simulation techniques. For these reasons, idealized intermolecular potential functions have the character of reference models in statistical thermodynamics, and their macroscopic properties are of broad interest in a variety of fields. They may be understood as virtual standard references in analogy to standard reference materials for experimental measurements and calibrations.[8] The Lennard-Jones potential describes interactions between spherical nonpolar particles, and is an

a)Electronic address: karsten.meier@hsuhh.de

important model in many applications of statistical thermodynamics.

This work describes an extensive molecular-dynamics simulation study of the transport coefficients of the Lennard-Jones model fluid.[9,10] In this first of a series of four papers, the results for the viscosity are presented. Subsequent papers deal with the self-diffusion coefficient, bulk viscosity, and thermodynamic properties.

Besides the self-diffusion coefficient, the viscosity η is the best investigated transport coefficient of the Lennard-Jones model fluid in molecular-dynamics simulations. However, the uncertainty of literature data is in part larger by up to two orders of magnitude than those commonly achieved in experiments for real fluids. In this work, we attempt to obtain viscosity data with small statistical uncertainties of only a few percent. This ambitious goal is achieved by performing very long simulation runs. Additionally, the kinetic-kinetic, kinetic-potential, and potential-potential viscosity contributions η_{kk}, η_{kp}, and η_{pp} are calculated at every simulated state point. These results characterize the behavior of the three viscosity contributions over a wide range of fluid states. Furthermore, the dependence of the viscosity and of the three viscosity contributions on density and temperature is examined in terms of the decay behavior of the shear-stress correlation functions.

This paper is organized as follows. The following section provides the theoretical background for the calculation of the viscosity in equilibrium molecular-dynamics simulations. Section III describes the simulation procedure and analysis of the results. In Sec. IV, an investigation of the influence of simulation parameters on the results for the viscosity is presented, and in Sec. V details of the simulations performed during the course of this work are provided. In Sec. VI, the viscosity data are discussed and compared with literature data of other research groups. In Secs. VII and VIII, the temperature and density dependence of the viscosity and the three viscosity contributions are discussed. Finally, an interpretation of the viscosity and the three viscosity contributions in Sec. IX in terms of shear-stress correlation functions provides insights into the momentum-transport mechanisms on the molecular scale.

II. THEORETICAL BACKGROUND AND SIMULATION METHODOLOGY

There are two different approaches to calculate the viscosity by molecular-dynamics simulations: either by time-correlation function theory employing the Green-Kubo integral formulas or Einstein relations in equilibrium simulations, or by nonequilibrium molecular dynamics. Many nonequilibrium techniques are described in the literature.[11–14] Although usually being considered as more efficient from a computational point of view than the application of time-correlation function theory in equilibrium simulations, nonequilibrium molecular-dynamics simulations encompass conceptual problems that make the rigorous analysis and interpretation of the results difficult. For example, the artificial removal of heat from a system with thermostating algorithms,[15] extrapolation of simulation results to thermodynamic equilibrium,[16] or introduction of periodic effects by the often employed Lees-Edwards boundary conditions[17] are still under discussion. Moreover, only one transport coefficient can be computed from a nonequilibrium simulation run, whereas equilibrium molecular dynamics is inherently a multiproperty method. In principle, all thermodynamic properties and transport coefficients can be computed at the same state point from a single simulation run, so that consistent data sets can be generated over wide ranges of thermodynamic states. For these reasons, equilibrium molecular-dynamics simulations were chosen for this work.

In time-correlation function theory, the viscosity is given by the Green-Kubo integral formula[18,19]

$$\eta = \frac{V}{kT}\int_0^\infty \langle \tau_{\alpha\beta}(t_0)\tau_{\alpha\beta}(t)\rangle dt \tag{1}$$

or equivalently by the Einstein relation[20]

$$\eta = \frac{V}{2kT}\lim_{t\to\infty}\frac{d}{dt}\left\langle\left[\frac{m}{V}\sum_{i=1}^{N}\left[v_{i,\alpha}(t)r_{i,\beta}(t) - v_{i,\alpha}(t_0)r_{i,\beta}(t_0)\right]\right]^2\right\rangle. \tag{2}$$

In these equations, V stands for the volume, k is the Boltzmann constant, T is the thermodynamic temperature, N is the number of particles, and m denotes the particle mass. The vector components $r_{i,\beta}$ and $v_{i,\alpha}$ represent the Cartesian components of the position and velocity vector of particle i, $\tau_{\alpha\beta}$ denotes an off-diagonal element of the stress tensor, and t is time. The angular brackets indicate an equilibrium ensemble average over short trajectory sections of the phase-space trajectory of the system with time origins t_0. In both cases, averaging over independent tensor elements, e.g., τ_{xy}, τ_{xz}, and τ_{yz}, can be used to reduce the statistical uncertainty of the viscosity data. The Green-Kubo integral formula determines the viscosity as the integral of the shear-stress correlation function $\langle \tau_{\alpha\beta}(t_0)\tau_{\alpha\beta}(t)\rangle$, whereas the Einstein relation relates the viscosity to the slope of a generalized mean-squared displacement function in the long-time limit $t\to\infty$. The generalized displacement function is proportional to the displacement of the center of the α component of the total-momentum vector of the system in the direction β. From a mathematical point of view, both the Green-Kubo integral formula, Eq. (1), and the Einstein relation, Eq. (2), are completely equivalent,[21] and could in principle be used to determine the viscosity.

In molecular-dynamics simulations with periodic boundary conditions, the Einstein relation cannot be applied directly because it assumes implicitly continuous particle trajectories that are unaffected by periodic boundary conditions.[21–23] Since the trajectories in a finite-system simulation with periodic boundary conditions are discontinuous whenever a particle leaves or enters the simulation box, the generalized displacement function must be calculated in a different way. An alternative way to calculate the generalized displacement function was suggested by Haile[21] and used by Rowley and Painter[24] in their study on the viscosity of the

Lennard-Jones fluid. The generalized displacement function is related to the time integral of the shear stress by

$$\frac{m}{V}\sum_{i=1}^{N}\left[v_{i,\alpha}(t)r_{i,\beta}(t)-v_{i,\alpha}(t_0)r_{i,\beta}(t_0)\right]=\int_0^t\tau_{\alpha\beta}(t)dt. \tag{3}$$

As the molecular expression for the shear stress is a function of the distances between all pairs of particles, their time evolution is in fact continuous if periodic boundary conditions and the minimum image convention are employed in a simulation. Therefore, Eq. (3) provides an indirect way to calculate the generalized displacement function for the viscosity. If it is inserted into Eq. (2), the Einstein relation reads

$$\eta=\frac{V}{2kT}\lim_{t\to\infty}\frac{d}{dt}\left\langle\left[\int_0^t\tau_{\alpha\beta}(t)dt\right]^2\right\rangle. \tag{4}$$

A more detailed discussion of this issue was given by Erpenbeck.[22]

The molecular expression for an off-diagonal element of the shear-stress tensor in terms of the particle positions and velocities is given by[25]

$$\tau_{\alpha\beta}=\underbrace{-\frac{1}{V}\sum_{i=1}^{N}mv_{i,\alpha}v_{i,\beta}}_{\tau_{\alpha\beta,\mathrm{k}}}\underbrace{-\frac{1}{V}\sum_{i=1}^{N-1}\sum_{j=i+1}^{N}r_{ij,\alpha}F_{ij,\beta}}_{\tau_{\alpha\beta,\mathrm{p}}}, \tag{5}$$

where $r_{ij,\alpha}$ is the α component of the distance vector between particles i and j and $F_{ij,\beta}$ is the β component of the force of particle i acting on particle j. The first term is the kinetic contribution $\tau_{\alpha\beta,\mathrm{k}}$, and the second term is the potential contribution $\tau_{\alpha\beta,\mathrm{p}}$ to the shear stress. When the separation of the shear stress, Eq. (5), is inserted into Eqs. (1) or (4), a subdivision of the viscosity into three different contributions is introduced:

$$\eta(\rho,T)=\eta_{\mathrm{kk}}(\rho,T)+\eta_{\mathrm{kp}}(\rho,T)+\eta_{\mathrm{pp}}(\rho,T). \tag{6}$$

After the brackets are multiplied out, the kinetic-kinetic, kinetic-potential, and potential-potential contributions to the viscosity are obtained as

$$\eta_{\mathrm{kk}}=\lim_{t\to\infty}\frac{V}{2kT}\frac{d}{dt}\left\langle\left[\int_{t_0}^t\tau_{\mathrm{xy,k}}(t)dt\right]^2\right\rangle, \tag{7}$$

$$\eta_{\mathrm{kp}}=\lim_{t\to\infty}\frac{V}{kT}\frac{d}{dt}\left\langle\left[\int_{t_0}^t\tau_{\mathrm{xy,k}}(t)dt\right]\left[\int_{t_0}^t\tau_{\mathrm{xy,p}}(t)dt\right]\right\rangle, \tag{8}$$

$$\eta_{\mathrm{pp}}=\lim_{t\to\infty}\frac{V}{2kT}\frac{d}{dt}\left\langle\left[\int_{t_0}^t\tau_{\mathrm{xy,p}}(t)dt\right]^2\right\rangle. \tag{9}$$

The three viscosity contributions depend on temperature as well as on density and are in general all nonzero. In the zero-density limit, the kinetic-kinetic contribution η_{kk} becomes

$$\lim_{\rho\to0}\eta_{\mathrm{kk}}(\rho,T)=\eta_0(T), \tag{10}$$

in which η_0 is the viscosity in the limit of zero density according to the Chapman-Enskog solution to the Boltzmann equation.[1] The contributions η_{kp} and η_{pp} are zero in this limit because the potential shear stress becomes zero.

Contrary to thermodynamic properties of monatomic fluids such as pressure or isochoric heat capacity, the viscosity cannot be divided into pure kinetic and potential parts, but contains cross contributions. This is a consequence of the fact that the kinetic and potential shear stresses are instantaneously uncorrelated, but at not too large time separations they are strongly correlated. Hence, in general there is a nonzero kinetic-potential contribution to the viscosity.

In the literature, other subdivisions of the viscosity have been proposed. Sharma[26] and Stassen and Steele[27,28] suggested extensions of the subdivision of the shear-stress correlation function introduced above, in which the contributions are based on the kind and number of particles involved in the correlations. Sharma introduced a single-particle shear stress as the sum of all terms involving one particle and separated the shear-stress correlation function into autocorrelations of particles with themselves and cross correlations between different particles. This subdivision was examined at one state point of the Lennard-Jones model fluid close to its triple point. Stassen and Steele separated the kinetic-potential and potential-potential parts of the shear stress correlation function into two- and three-body and two-, three-, and four-body contributions depending on the number of particles involved in the correlations. They investigated their subdivision scheme at five states on a subcritical isotherm and the same state point that was used by Sharma. These results supplement the investigations of the subdivision of the viscosity undertaken in this work and will turn out to be useful when discussing the dependence of the shear-stress correlation function on temperature and density in Sec. IX.

In the remainder of this paper, reduced quantities denoted by a superscript asterisk "*" are used, e.g., $T^*=Tk/\varepsilon$, $\rho^*=\rho\sigma^3$, $t^*=t\sqrt{\varepsilon/m}/\sigma$, $r^*=r/\sigma$, $\tau^*=\tau\sigma^3/\varepsilon$, and $\eta^*=\eta\sigma^2/\sqrt{m\varepsilon}$, where ε and σ are the energy and length parameters of the Lennard-Jones potential.

III. SIMULATION ANALYSIS

All simulations of this work were carried out in the classical molecular-dynamics ensemble at constant $NVE\mathbf{MG}$. Besides the number of particles N, the volume V, and the internal energy of the system E, the total momentum of the system $\mathbf{M}$ and the quantity $\mathbf{G}$, which is related to the initial value of the center of mass of the system, are kept constant during the simulation.[29,30] The velocity-Verlet algorithm was used to integrate the equations of motion, and the usual periodic boundary conditions and minimum image convention were applied.[25] The simulation software is based on FORTRAN codes provided on microfiche as attachments to the book of Allen and Tildesley.[25] After a simulation run, several separate analysis programs were used to compute thermodynamic properties, time-correlation functions and generalized mean-squared displacements from the data stored during the simulation. In a subsequent analysis step, the viscosity contributions were deduced from their corresponding Einstein relations, Eqs. (7)–(9), as the long-time limit of the slopes of the generalized mean-squared displacement functions.

TABLE I. Simulation data for the viscosity and viscosity contributions at the state point ($T^*=0.722$, $\rho^*=0.8442$) close to the triple point of the Lennard-Jones model fluid. The simulations extended over 10×10^6 time steps.

N	r_{cut}^*	T^*	η_{kk}^*	η_{kp}^*	η_{pp}^*	η^*
108	2.5	0.731 262	0.047 86	0.052 22	2.884	2.984
256	3.25	0.733 052	0.049 99	0.061 19	2.994	3.105
500	4.0	0.722 001	0.049 37	0.061 32	3.077	3.188
864	5.0	0.721 355	0.049 59	0.056 21	3.208	3.314
2048	5.5	0.721 444	0.051 49	0.058 40	3.114	3.224
4000	5.5	0.722 109	0.050 97	0.061 46	3.163	3.275
4000[a]	5.5	0.722 096	0.050 60	0.063 30	3.132	3.246
1372	2.5	0.723 441	0.048 85	0.072 49	3.156	3.277
1372	2.75	0.732 155	0.051 65	0.063 07	3.156	3.271
1372	3.0	0.712 572	0.049 90	0.063 45	3.182	3.295
1372	3.25	0.730 478	0.050 41	0.066 61	3.107	3.224
1372	3.5	0.717 710	0.050 00	0.066 14	3.153	3.269
1372	3.75	0.719 279	0.050 30	0.059 18	3.128	3.237
1372	4.0	0.721 561	0.051 12	0.054 42	3.140	3.245
1372	4.25	0.718 948	0.049 29	0.058 98	3.091	3.199
1372	4.5	0.721 795	0.050 23	0.076 37	3.123	3.249
1372	4.75	0.721 195	0.050 73	0.058 40	3.082	3.191
1372	5.0	0.721 228	0.050 85	0.058 04	3.113	3.222
1372	5.25	0.722 564	0.050 39	0.055 81	3.055	3.161
1372	5.5	0.722 266	0.050 67	0.060 13	3.174	3.284

[a]25×10^6 time steps.

The viscosity data were obtained as the sum of the three viscosity contributions according to Eq. (6).

To determine the time-correlation functions and generalized displacement functions, time origins were taken at equally spaced intervals along the simulated phase-space trajectory of the system. Starting at the time origins, phase variables were correlated with their values at the origins, and generalized displacement functions were computed along short sections of the phase-space trajectory by numerical integration of the corresponding shear-stress contributions using Simpson's rule. The lengths of the trajectory sections were chosen so that all relevant correlations decayed to zero and the linear regime of the generalized displacement functions was evident within the length of the sections. The lengths of the trajectory sections depended on the temperature and density of the state point. The long-time limit of the slope of the generalized mean-squared displacement functions is obtained from a least-squares fit of a straight line to the linear regime of the plot.

Every simulation result is subject to statistical and systematic errors. Statistical errors in simple simulation averages were estimated by the method described by Allen and Tildesley,[25] which is originally due to Friedberg and Cameron.[31] Uncertainties of simulation results for the viscosity contributions were estimated from the quality of the fit of the straight line to the generalized mean-squared displacement function and from the scatter of the data along isotherms and isochors. In this work, uncertainties of the simulation results are not reported for every single state point, but are summarized for characteristic parts of the fluid region of the phase diagram.

IV. INFLUENCE OF SIMULATION PARAMETERS ON THE VISCOSITY

Systematic errors are caused, for example, by the potential truncation at the cutoff radius, finite-size effects due to the use of small particle numbers, numerical imprecisions in the integration of the equations of motion, or insufficient equilibration of the system before the production phase of a simulation. Systematic errors can be eliminated to some extent by a careful choice of the simulation parameters. Since it is not *a priori* known how the simulation parameters must be chosen, a systematic investigation of their influence on the results for macroscopic properties is required.

Before starting the production phase, every simulation was run over at least 100 000 time steps to attain thermodynamic equilibrium in the system. The step size for the velocity-Verlet integrator was set to $\Delta t^*=0.003$. Even extremely long simulations over 50×10^6 time steps at gaseous states could be run without rescaling the velocities in order to correct for small energy drifts as sometimes done by other authors.[25] The total energy of the system was always kept constant within two parts in 10^5. With these choices, it is ensured that both parameters do not significantly influence the results for the macroscopic properties of the system.

The influence of the cutoff radius r_{cut}^* and of the number of particles N on the viscosity and its three contributions were investigated at the state point ($T^*=0.722$, $\rho^*=0.8442$) close to the triple point of the Lennard-Jones model fluid ($T_{tr}^*=0.67$, $\rho_{tr}^*=0.8442$).[32] The viscosity at this state was studied often since the initial work by Levesque *et al.*[33] At the low temperature of this liquid state, the correlation functions decay extremely slowly, and thus the viscosity should be most difficult to obtain.

To examine the influence of the cutoff radius, several simulations with 1372 particles and different cutoff radii were performed. All simulations extended over 10×10^6 time steps. The results for the viscosity and the three viscosity contributions are reported in Table I. The data show no systematic dependence on the cutoff radius above $r_{cut}^*=4.5$. Consequently, the influence of the cutoff radius is negligible

TABLE II. Literature data for the viscosity of the Lennard-Jones fluid close to its triple point. Abbreviations: DT, difference in trajectories method; ER, Einstein relation method; GK, Green-Kubo integral method; LE, Lees-Edwards shear boundary conditions; OS, oscillating-shear perturbed-Hamiltonian method; TS, trajectory segments; WR, wall reservoir boundary conditions; MC-GO, Monte Carlo generated time origins.

Author	Year	Data	Method	Ensemble	N	r_{cut}^*	Sim. Length[a]	T^*	ρ^*	$\eta^{*,b}$
This work	2004	20	ER	*NVEMG*	256–4000	2.5–5.5	30 000–75 000	0.717–0.733	0.8442	3.258
Ashurst (Ref. 39)	1975	3	WR	···	108–324	c	464	0.722	0.8442	3.21
Erpenbeck (Ref. 34)	1988	2	GK	*NVT*	108, 864	2.5	MC-GO	0.722	0.8442	3.200
Evans (Ref. 40)	1981	1	LE	*NVT*	108, 256	2.5	up to 3640	0.722	0.8442	3.17
Evans (Ref. 36)	1989	1	LE	*NVT*	2048	3.5	120–560	0.722	0.8442	3.41
Ferrario (Ref. 52)	1991	7	GK	*NVT*	500–4000	2.5	1600–18 000	0.725	0.8442	3.24
Heyes (Ref. 41)	1980	1	DT	*NVT*	108	2.5	20 TS	0.722	0.8442	2.7
Heyes (Ref. 44)	1983	1	DT	*NVEMG*	256	2.5	150	0.73	0.8442	3.03
Heyes (Ref. 45)	1986	1	DT	*NVT*	256	2.5	200 TS	0.722	0.8442	3.1
Heyes (Ref. 42)	1988	3	GK	*NVT*	108–500	c	3295–8780	0.72	0.848	3.4
Heyes (Ref. 43)	1990	1	GK	*NVT*	256	2.5	1500	0.722	0.8442	3.74
Hoover (Ref. 46)	1980	1	WR	···	864	2.5	700	0.715	0.8442	3.0
		1	OS	···	108	2.5	0.03–7.7	0.722	0.8442	3.18
Levesque (Ref. 33)	1973	1	GK	*NVEMG*	864	c	466	0.722	0.8442	4.0
Levesque (Ref. 47)	1987	5	GK	*NVEMG*	108–864	c	11–88	0.715–0.728	0.8442	3.8
Pollock (Ref. 48)	1980	2	GK	c	256, 500	c	c	0.722	0.8442	3.2
Schoen (Ref. 49)	1985	1	GK	*NVEMG*	500	2.5	232	0.73	0.8442	3.19
Sharma (Ref. 37)	1991	4	GK	*NVT*	32–500	1.6, 2.5	80–400	0.72	0.844	3.34
Sharma (Ref. 26)	1994	5	GK	*NVT*	32–864	1.6, 2.5	80–400	0.72	0.84	3.402
Singer (Ref. 50)	1980	1	DT	*NVE*	256	c	100 TS	0.722	0.8442	2.42
Stassen (Ref. 27)	1995	1	GK	*NVEMG*	256	3.4	325	0.72	0.8445	3.297
Trozzi (Ref. 51)	1984	2	WR	···	180, 384	2.5, 3.5	c	0.722	0.8442	3.26

[a]Values of the simulation length are given in reduced time units.
[b]Extrapolation to infinite system size or datum from the simulation with the largest system.
[c]Not reported by the authors.

if it is chosen larger than 4.5. Six additional simulations over 10×10^6 time steps were carried out with 108–4000 particles to investigate the influence of the number of particles. After 10×10^6 time steps, the simulation with 4000 particles was continued up to 25×10^6 time steps. In simulations with 1372 or more particles, the cutoff radius was set to $r_{cut}^*=5.5$, while in simulations with fewer particles it was chosen slightly smaller than half the box length. The results of these simulations are also reported in Table I.

Details of the literature viscosity data are collected in Table II. Data for the viscosity contributions were reported by Erpenbeck[34] and Stassen and Steele.[27] Erpenbeck[35] reported eight data, from which six data were derived from simulations with a modified Lennard-Jones potential. In order to minimize the influence of the cutoff radius, the long-range attractive part of the Lennard-Jones potential was replaced by a cubic polynomial function that decays continuously to zero. Evans *et al.*[36] pointed out that the modification of the intermolecular potential function results in macroscopic thermodynamic properties and transport coefficients that deviate significantly from the corresponding properties of the original potential. Hence, these data cannot be compared with those data sets obtained with the original Lennard-Jones potential and are excluded from further considerations. Sharma and Woodcock[37] and Sharma[26] presented additional data, which were obtained by the Green-Kubo integral formulas, but they used a different cutoff model to compute the shear-stress correlation functions. These data are also not taken into account in the following discussion. Heyes[38] provided 17 nonequilibrium data that were not extrapolated to zero shear rate and can therefore not be compared with the present data.

Figure 1 depicts the results for the viscosity and the viscosity contributions as a function of the inverse number of particles at this state point and includes literature data for these quantities. The viscosity is dominated by the η_{pp}^* contribution so that η^* closely resembles the behavior of η_{pp}^*. All three contributions increase with the number of particles. The contribution η_{kk}^* is the smallest and shows the weakest dependence on the number of particles. The cross contribution η_{kp}^* shows the highest scatter, but the overall tendency to increase with the number of particles is evident. It is about 20% larger than η_{kk}^*. Altogether, both contributions amount to less than 5% of the total viscosity.

Comparing the present results with literature data, we note two groups of the latter. The bulk of them were derived from short simulation runs such as those of Ashurst and Hoover,[39] Evans,[40] Heyes *et al.*,[41–45] Hoover *et al.*,[46] Levesque *et al.*,[33] Levesque and Verlet,[47] Pollock,[48] Schoen and Hoheisel,[49] Sharma and Woodcock,[37] Sharma,[26] Singer *et al.*,[50] Stassen and Steele,[27] and Trozzi and Cicotti.[51] Therefore, the uncertainty and scatter of these data is quite high. Some of these results agree well with the data of this work. A second group includes data sets which were derived from long simulation runs. These are the data of Erpenbeck,[34] Evans,[36] and Ferrario *et al.*[52] Their results agree well with those of this work. The few literature data for the viscosity contributions yield only little additional insight. The potential-potential contribution η_{pp}^* follows the corresponding data for the total viscosity, while the data for the cross contribution η_{kp}^* are much lower than the present data for this contribution. Good agreement is found between the present and the literature data for the kinetic-kinetic contribution η_{kk}^*.

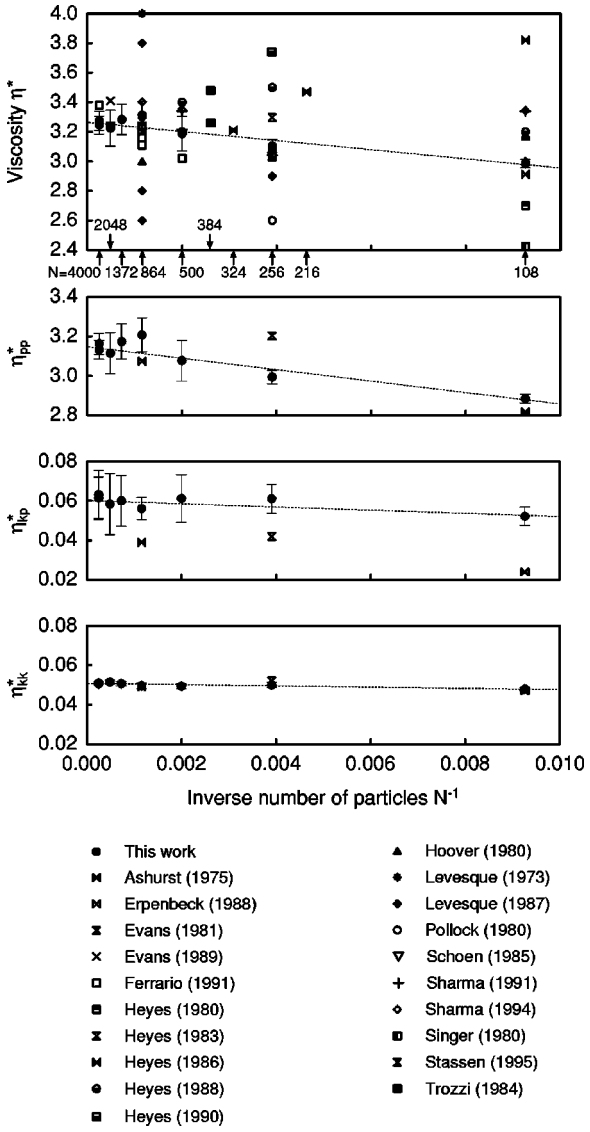

FIG. 1. Present simultion data and literature data for the viscosity contributions η^*_{kk}, η^*_{kp}, and η^*_{pp}, and the viscosity η^* at the state point ($T^*=0.722$, $\rho^*=0.8442$) as a function of the inverse number of particles. Error bars designate the uncertainty of the present data. The dashed lines represent weighted linear least-squares fits to the present data.

A linear dependence on the inverse number of particles is assumed for the extrapolation of the data for the viscosity and viscosity contributions at ($T^*=0.722$, $\rho^*=0.8442$) to infinite system size ($N^{-1}\rightarrow 0$). From a weighted linear least-squares fit to the present data, the following estimates for the infinite system size limit are derived

$$\eta^* = 3.258 \pm 0.033,$$

$$\eta^*_{kk} = 0.05079 \pm 0.00033,$$

$$\eta^*_{kp} = 0.06023 \pm 0.0042,$$

$$\eta^*_{pp} = 3.147 \pm 0.028.$$

Erpenbeck[34] estimated the value $\eta^*=3.345\pm0.068$ for the infinite system size viscosity from a weighted linear least-squares fit to his data for a modified Lennard-Jones potential. To account for the difference in the potential function, a correction was applied to the data before the fit. Schoen and Hoheisel[23,49] reported the value $\eta^*=3.18\pm0.15$ for a simulation with 500 particles. They observed no dependence of their data on the number of particles within the uncertainty of the data for systems of more than 256 particles. Therefore, this value represents the viscosity for the infinite system size within the quoted uncertainty. The present value agrees with these two literature results within the combined uncertainties.

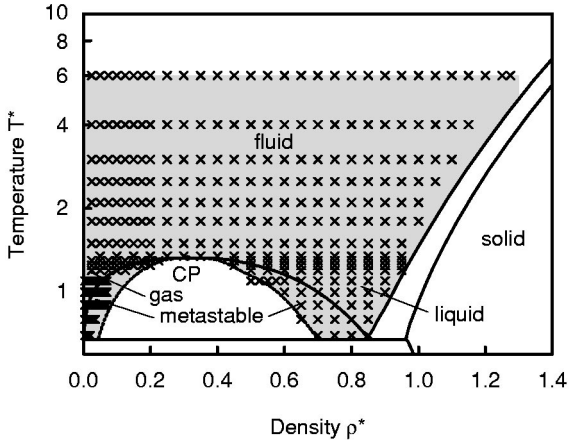

FIG. 2. Distribution of simulated state points in the T^*, ρ^* plane.

To conclude, for the target system size of 1372 particles employed in the present simulations the statistical uncertainty of the data is larger than their dependence on the number of particles, even for long simulation runs over 10×10^6 time steps. Therefore, the dependence of the simulation data on the number of particles for the viscosity is negligible.

V. SIMULATION DETAILS

Extensive equilibrium molecular-dynamics simulations were carried out to determine the transport coefficients of the Lennard-Jones model fluid over a wide range of fluid states along 16 isotherms on 351 state points. Input internal energies for a given temperature T^* and density ρ^* were calculated from the fundamental equation of state of Mecke *et al.*[53] All simulations were performed with 1372 particles and a time step size of $\Delta t^*=0.003$. After an equilibration phase of 100 000 up to 300 000 time steps, the production phase of the simulations proceeded over 1.5 to 2×10^6 time steps. The cutoff radius r^*_{cut} depended on the density of the state point. It was set to $r^*_{cut}=5.0$ for $\rho^*>1.0$, 5.5 for $0.6<\rho^*\leqslant1.0$, and 6.5 for $\rho^*\leqslant0.6$.

The distribution of the simulated state points relative to the phase boundaries is shown in Fig. 2. The simulations extend over a wide range of the fluid region of the phase diagram from the low-density gas to the compressed liquid close to the freezing line with temperatures between $T^*=0.7$ and 6.0. Metastable vapor and liquid states were also included. However, state points that apparently lie in the unstable region were not considered. Unstable states were identified by inspection of simulated heat capacities and isentropic compressibilities. If these thermodynamic state variables

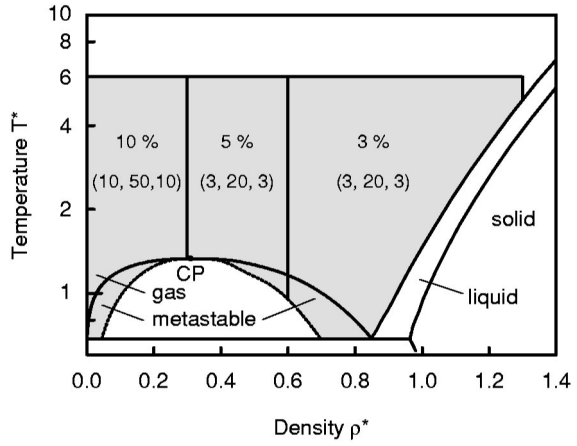

FIG. 3. Estimated uncertainties of the data from the first series of simulations for the viscosity η^* and for the viscosity contributions η^*_{kk}, η^*_{kp}, and η^*_{pp} in parentheses.

showed unphysical behavior or values, e.g., either negative or very large positive values, a state point was considered to lie in the unstable region. At every simulated state point, several thermodynamic properties and the transport coefficients viscosity, bulk viscosity, and the self-diffusion coefficient, as well as the three viscosity contributions, were evaluated. While the viscosity is the subject of this paper, the results for the bulk viscosity, the self-diffusion coefficient, and thermodynamic properties are reported in separate publications.[54–56]

In addition to this large body of simulations, two further simulation series were carried out. One series repeated simulations at low-temperature gaseous states between the temperatures $T^*=0.7$ and 1.2 at 39 state points. The production phases of these simulations extended over 50×10^6 time steps. These simulations were performed to determine the behavior of the viscosity and bulk viscosity in this state region more precisely. Another 11 simulations extending over 10×10^6 time steps were mainly performed on the near-critical isotherm $T^*=1.35$ to determine the behavior of the bulk viscosity and thermal conductivity in the vicinity of the critical point.

At every simulated state point, the generalized mean-squared displacements and shear-stress correlation functions were computed. The parameters for the computation of both functions were the same at every state point. Every fifth time step was taken as a new time origin. The data for the viscosity contributions were derived from the generalized displacement functions as described in Sec. III, and the total viscosity was then obtained as the sum of the three contributions. All simulation data of this work and colored versions of the figures of this paper were deposited in the electronic archive of this journal[57] and in the electronic archive of the NIST Physical and Chemical Properties Division.[58]

The uncertainties of the viscosity data of the first simulation series are summarized in Fig. 3. They are estimated to be 3% at high densities above $\rho^*=0.6$, 5% for densities between $\rho^*=0.3$ and $\rho^*=0.6$ and 10% for densities below $\rho^*=0.3$. The uncertainties of the viscosity contributions depend on the contribution as well as on density. The η^*_{kk} and η^*_{pp} data have uncertainties of 3% at high densities, while at densities below $\rho^*=0.3$ in the gas region the uncertainties increase up to 10%. The data for η^*_{kp} have higher uncertainties of about 20% over almost the entire range of density and temperature. At low temperatures in the gas region, the uncertainty of the data is even higher, with up to 50%.

The uncertainty of the data of the second simulation series at gaseous densities is lower. The viscosity data and η^*_{kk} data have uncertainties of about 4%, whereas the uncertainties of the data for η^*_{kp} and η^*_{pp} are estimated to be 30% and 1%, respectively.

VI. COMPARISON WITH LITERATURE DATA

Table III summarizes the available literature data sets for the viscosity of the Lennard-Jones model fluid with their characteristic simulation parameters. Holian and Evans[61] applied a modified Lennard-Jones potential in their simulations, which results in macroscopic properties different from those of the application of the original Lennard-Jones potential. Thus their data are excluded from further consideration. In most studies, the viscosity was obtained from the time integral of the shear-stress correlation function by use of the Green-Kubo integral formula. Besides the data of this work, only the data of Rowley and Painter were obtained by the Einstein relation. Nonequilibrium molecular dynamics was used by Ashurst and Hoover[39] and Heyes.[42,62] Additionally, Heyes[45] carried out nonequilibrium simulations using the difference in trajectories method, but the data were not reported in the publication. Almost all literature simulation studies applied small cutoff radii between $r^*_{cut}=2.5$ and 3.5, and only very few simulations were conducted with more than 500 particles, whereas the present simulations were performed with cutoff radii between $r^*_{cut}=5.0$ and 6.5 and 1372 particles. An important indicator for the quality of simulation data is the simulation length since it determines the statistical uncertainty of the data. The simulations of Hammonds and Heyes,[63] Heyes *et al.*,[42,62,64] Michels and Trappeniers,[65] and Rowley and Painter[24] extend over redundant periods similar to or longer than those in the simulations of this work.

The distribution of the literature viscosity data in the T^*, ρ^* plane is given in Fig. 4. The available literature data concentrate in the high-density liquid region below the $T^*=3.0$ isotherm. The data sets of Heyes[42] and Rowley and Painter[24] are the most comprehensive and cover a state region similar to that of this work. The data of Heyes extend to higher temperatures, but do not cover low-density gaseous states. The simulations of Rowley and Painter cover the temperature range from $T^*=0.8$ to 4.0 and extend from low-density gaseous states to the density $\rho^*=1.0$. Rowley and Painter included state points in the metastable and unstable region of the phase diagram. Data in the gas region at supercritical temperatures were reported by Michels and Trappeniers.[65] They also investigated the subdivision of the viscosity into the three contributions. These data were obtained from very long simulations extending over 150 000 reduced time units and supplement the subcritical low-density data from the second simulation series of this work.

TABLE III. Literature data sets for the viscosity of the Lennard-Jones model fluid. Abbreviations: DT, difference in trajectories method; ER, Einstein relation; GK, Green-Kubo integral; LE, Lees-Edwards shear boundary conditions; WR, wall reservoir boundary conditions. Literature data for the viscosity already listed in Table II are not considered here.

Author	Year	Data	Method	Ensemble	N	r_{cut}^*	T^*	ρ^*	Sim. Length[a]
This work	2004	343	ER	*NVE***MG**	1372	5.0–6.5	0.7–6.0	0.005–1.275	4500–6000
This work	2004	39	ER	*NVE***MG**	1372	6.5	0.7–1.2	0.005–0.15	150000
This work	2004	11	ER	*NVE***MG**	1372	6.5	1.35	0.05–0.45	30000
Ashurst (Ref. 39)	1975	39	WR[b]	*NVE*	108–324	c	0.7–30.0	0.25–1.4	464
Borgelt (Ref. 59)	1990	46	GK	*NVE***MG**	108	2.5	0.66–2.94	0.78–0.8415	371
Canales (Ref. 60)	1999	3	GK/ER	*NVT*	668	2.71, 3.11[d]	0.53, 1.89	0.756, 1.143	554–1203
Hammonds (Ref. 63)	1988	51	GK	*NVE***MG**/*T*	108–500	2.5[e]	0.72–10.0	0.4–1.18	3000–14000
Heyes (Ref. 44)	1983	49	DT	*NVE***MG**	256	2.5	0.68–4.58	0.2–1.13	150
Heyes (Ref. 62)	1987	16	LE	*NVT*	108–2048	c	1.4562	0.1–1.0	100–9000
Heyes (Ref. 42)	1988	208	GK	*NVT*	108–500	c	0.72–10.0	0.2–1.22	417–9500
		87	LE	*NVT*	256	c	1.45–10.0	0.3–1.22	278, 1460
Heyes (Ref. 43)	1990	25	GK	*NVT*	256	2.5	0.722–6.0	0.4–1.4	1500
Heyes (Ref. 64)	1993	4	GK	*NVE***MG**	256	2.5	0.707–6.02	0.5–1.0	655–17082
Holian (Ref. 61)	1983	1	LE	*NVT*	108	1.24[f]	2.75	0.7	60–900
		3	GK	*NVE***MG**	108–4000	1.24[f]	2.75	0.7	45–98
Levesque (Ref. 47)	1987	4	GK	*NVE***MG**	108, 864	c	2.725–2.803	0.962–1.113	11–88
Michels (Ref. 65)	1985	36	GK	*NVE***MG**	108	2.5	1.3–10.0	0.05–0.3	9120–151200
Rowley (Ref. 24)	1997	171	ER	*NVT*	256	3.5	0.8–4.0	0.05–1.0	182–6063
Schoen (Ref. 49)	1985	13	GK	*NVE***MG**	32–2048	2.5	0.68–4.42	0.5–1.113	232–928
Schoen (Ref. 23)	1986	32	GK	*NVE***MG**	500	2.5	0.68–4.0	0.45–0.85	464
Sharma (Ref. 26)	1994	2	GK	*NVT*	108	2.5	0.59, 0.61	1.0, 1.21	320
Stassen (Ref. 27)	1995	5	GK	*NVE***MG**	256	3.4–5.3	1.26	0.211–0.8445	325

[a]Values of the simulation length are given in reduced time units.
[b]Nonequilibrium data not extrapolated to zero shear rate.
[c]Not reported by the authors.
[d]According to Fig. 1 in Ref. 60.
[e]According to Fig. 1 in Ref. 63.
[f]Modified Lennard-Jones potential.

Schoen[23] explored the temperature dependence of viscosity isochors at high densities.

In Figs. 5 and 6, results for the viscosity η^* and viscosity contributions η_{kk}^*, η_{kp}^*, and η_{pp}^* are shown for the subcritical isotherm $T^*=1.3$ and the supercritical isotherm $T^*=2.5$. Also shown are literature data from different sources discussed above and the correlation of Rowley and Painter.[24] At high densities, the viscosity is dominated by the potential-potential contribution η_{pp}^*, while η_{kk}^* and η_{kp}^* contribute little. At low densities, the η_{pp}^* isotherms are relatively flat, but with increasing densities they become steeper and increase exponentially at high densities. The data for η_{pp}^* are very consistent over the whole density range. The kinetic-kinetic contribution η_{kk}^* yields the largest contribution to the total viscosity at low densities in the gas region, decreases with density, and becomes flat close to the freezing line. The data for this contribution are fairly consistent at intermediate and high densities, but show some scatter in the gas region. The kinetic-potential contribution η_{kp}^* shows a different behavior. At gaseous densities, it increases, reaches a maximum at intermediate densities, and decreases in the high density region. The cross contribution η_{kp}^* shows the largest scatter of the three viscosity contributions and is the most difficult to simulate accurately.

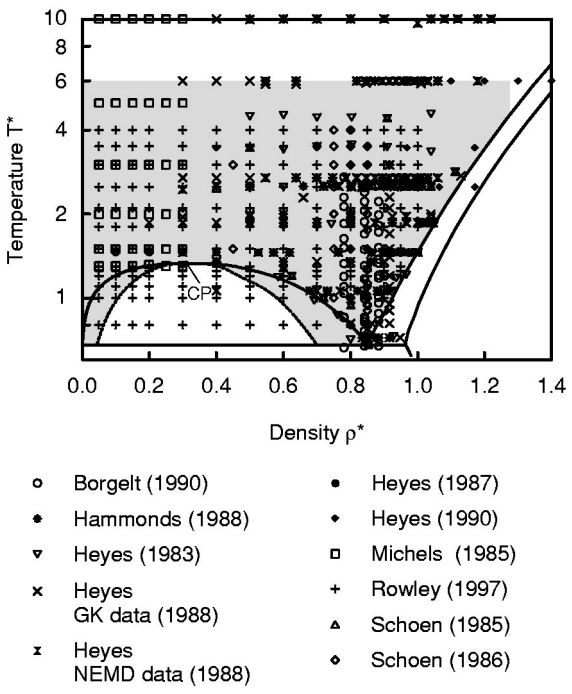

FIG. 4. Distribution of literature data for the viscosity η^* in the T^*, ρ^* plane. The shaded area is the state region considered in this work.

At liquid densities, the viscosity data of this work show less scatter than the data of Hammonds and Heyes,[63] Heyes,[42–44] Rowley and Painter,[24] Schoen and Hoheisel,[49] and Schoen[23] at liquid densities. Michels and Trappeniers[65] investigated the behavior of the three viscosity contributions on the isotherm $T^*=1.3$ up to the density $\rho^*=0.3$. Their data are almost indistinguishable from the present data for the three contributions and total viscosity, while the viscosity

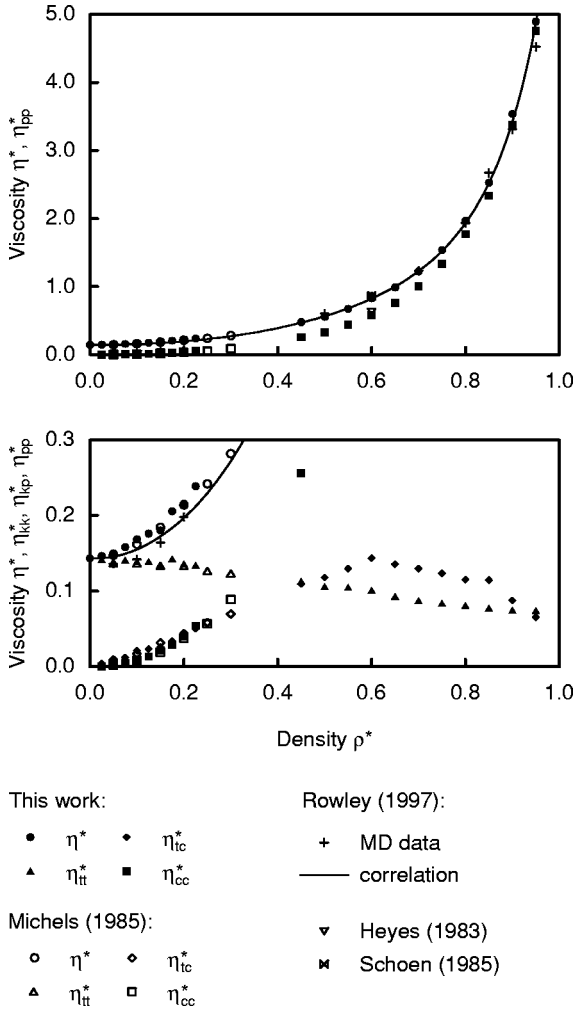

FIG. 5. The viscosity η^* and the viscosity contributions η^*_{kk}, η^*_{kp}, and η^*_{pp} along the subcritical isotherm $T^*=1.3$ as a function of density. Symbols at zero density denote the Chapman-Enskog solution to the Boltzmann equation.

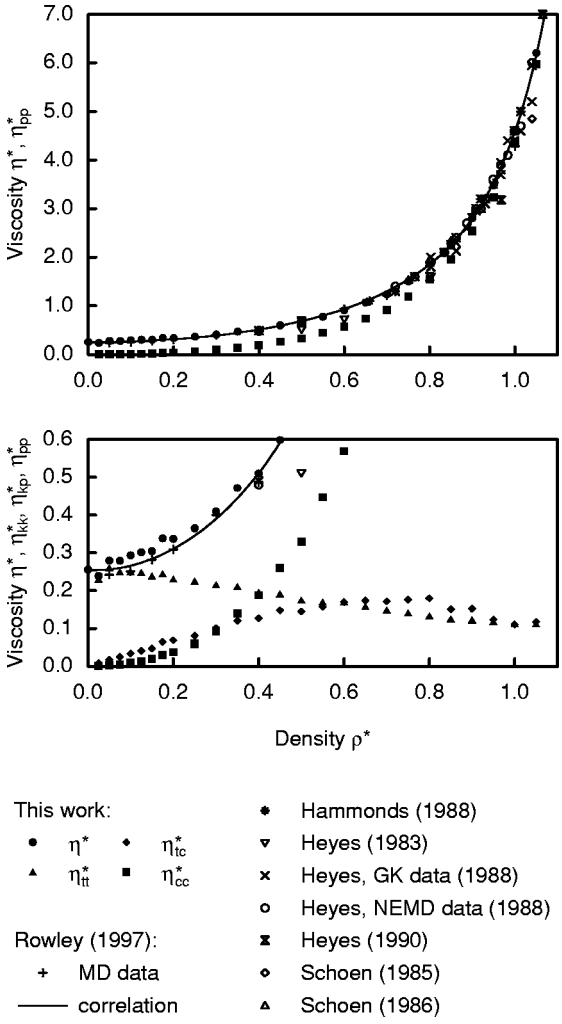

FIG. 6. The viscosity η^* and the viscosity contributions η^*_{kk}, η^*_{kp}, and η^*_{pp} along the supercritical isotherm $T^*=2.5$ as a function of density. Symbols at zero density denote the Chapman-Enskog solution to the Boltzmann equation.

data of Rowley and Painter lie below the present results. Furthermore, the present data extrapolate well into the zero-density limit. The correlation of Rowley and Painter[24] follows the present data well at high densities. However, this is surprising since it was fitted to only their own data. In the gas region, the data of this work lie above the correlation on both isotherms, suggesting that the correlation predicts gas viscosities that are too low.

VII. TEMPERATURE AND DENSITY DEPENDENCE OF THE VISCOSITY

Figure 7 gives an overview over all 16 simulated viscosity isotherms. The viscosity of the Lennard-Jones model fluid shows the typical temperature and density dependence known for real fluids. The isotherms intersect in the density range between $\rho^*=0.75$ and 0.8, which corresponds to ≈ 2.5 times the critical density. The intersection points mark a change in the temperature dependence of the viscosity. At lower densities, the viscosity increases with temperature, while it decreases at higher densities in the liquid region.

Another viewpoint is explored when the viscosity is plotted along isochors as a function of temperature. Figure 8 shows the viscosity for eight selected isochors between $\rho^*=0.45$ and 0.95 and the data of Schoen[23] on four isochors between $\rho^*=0.45$ and 0.85. The two lowest displayed isochors $\rho^*=0.45$ and 0.6 are almost parallel to the zero-density viscosity at supercritical temperatures. Thus, the residual viscosity, i.e., the viscosity minus the viscosity in the limit of zero density, depends only weakly on temperature. This observation agrees with the behavior of the viscosity of real fluids in this state region.[66]

The temperature dependence changes on the isochors $\rho^*=0.7$, 0.75, and 0.8. The viscosity decreases at low temperatures, reaches a minimum, and increases in the high-temperature region. This is the density range where the viscosity isotherms in Fig. 7 intersect. The temperature T^*_I for which $\partial\eta^*/\partial T^*_I=0$ is the inversion temperature. It marks a transition from gaslike ($T^*>T^*_I$) to liquidlike ($T^*<T^*_I$) viscous behavior. The inversion temperature is indicated by the dotted line in Fig. 8. It increases with density from approximately the critical temperature on the isochor $\rho^*=0.7$

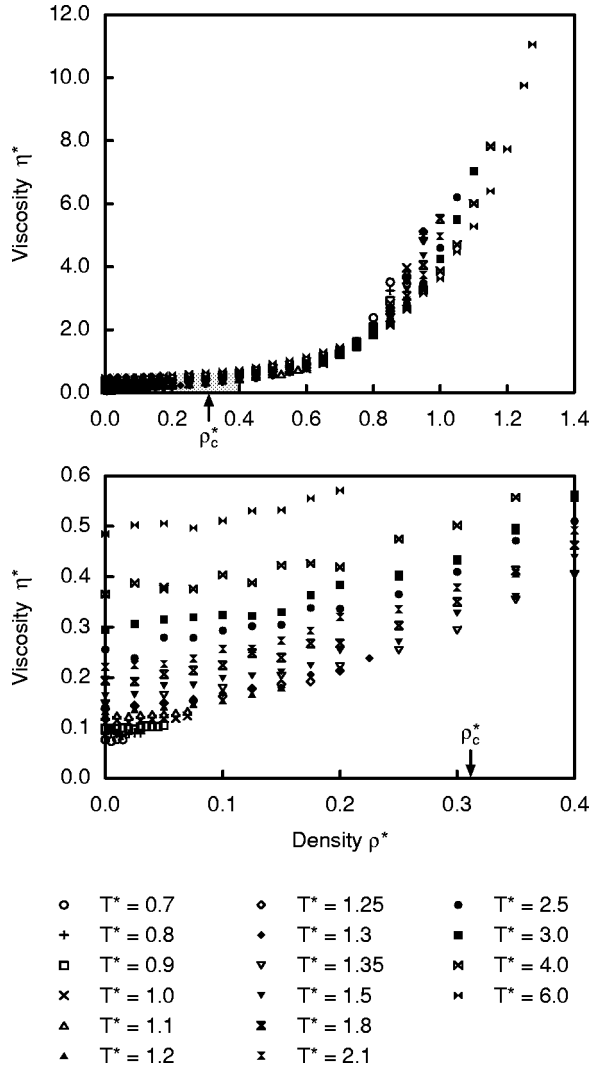

FIG. 7. The viscosity η^* for all simulated isotherms as a function of density. Symbols at zero density denote the Chapman-Enskog solution to the Boltzmann equation. The shaded area is enlarged in the bottom plot.

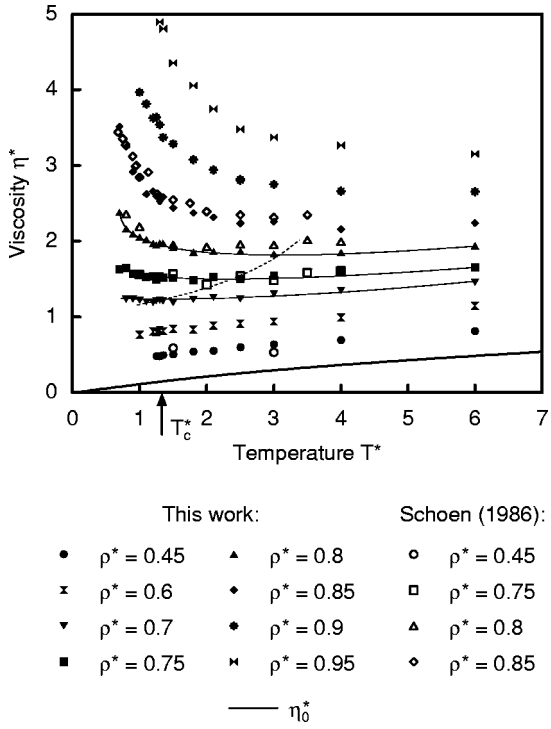

FIG. 8. The viscosity η^* for selected isochors as a function of temperature. Lines are drawn to guide the eye.

to about $T_I^* = 3.0$ on the isochor $\rho^* = 0.8$. From the density $\rho^* = 0.85$ on, the isochors show the typical behavior for the liquid region and decrease monotonically with temperature.

The data of Schoen[23] scatter higher than of the present results on the isochors $\rho^* = 0.45$ and 0.75. On the two higher isochors $\rho^* = 0.8$ and 0.85, the data of Schoen lie above the data of this work. Schoen's data suggest that the isochors $\rho^* = 0.8$ and 0.85 exhibit minima, but the present data support only the minimum on the isochor $\rho^* = 0.8$. A comparison of the parameters of Schoen's and the present simulations (see Table III) suggests that the present data are more accurate. Schoen reports the statistical uncertainty of his data to be about 3%–5%, while the present data have an uncertainty of 3%.

VIII. THE VISCOSITY CONTRIBUTIONS

It is worthwhile to examine the temperature and density dependence of the three viscosity contributions in detail, because they have not been computed before as comprehensively as in this work.

Figure 9 displays the density dependence of the kinetic-kinetic viscosity contribution at all 16 simulated temperatures. The isotherms are clearly distinguishable and do not intersect. Overall, η_{kk}^* decreases with density along the isotherms. The decrease becomes stronger with temperature. Weak density dependences are observed in the gas region

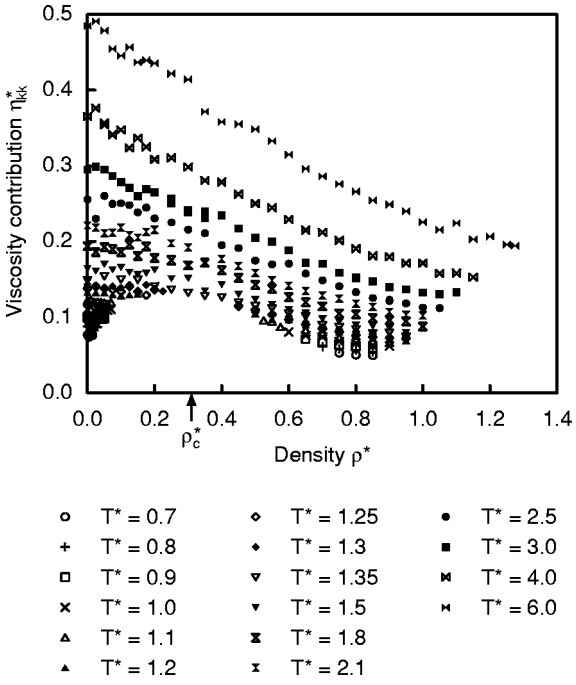

FIG. 9. The kinetic-kinetic viscosity contribution η_{kk}^* for all simulated isotherms as a function of density.

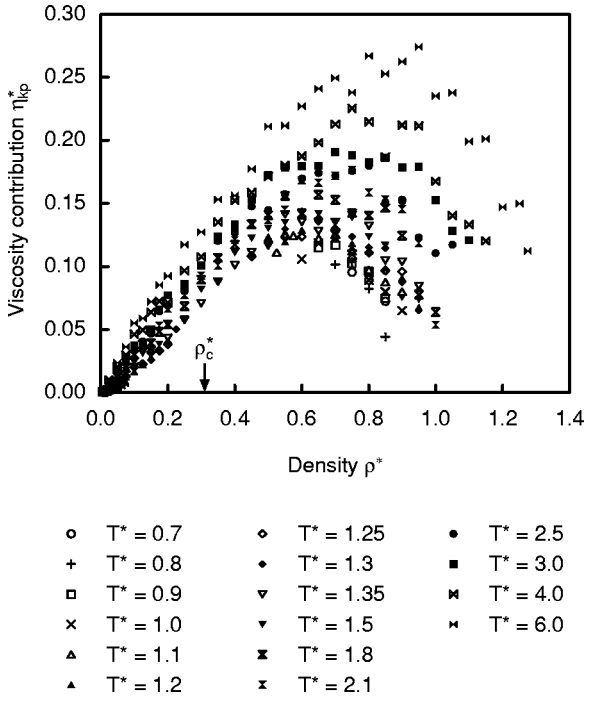

FIG. 10. The kinetic-potential viscosity contribution η^*_{kp} for all simulated isotherms as a function of density.

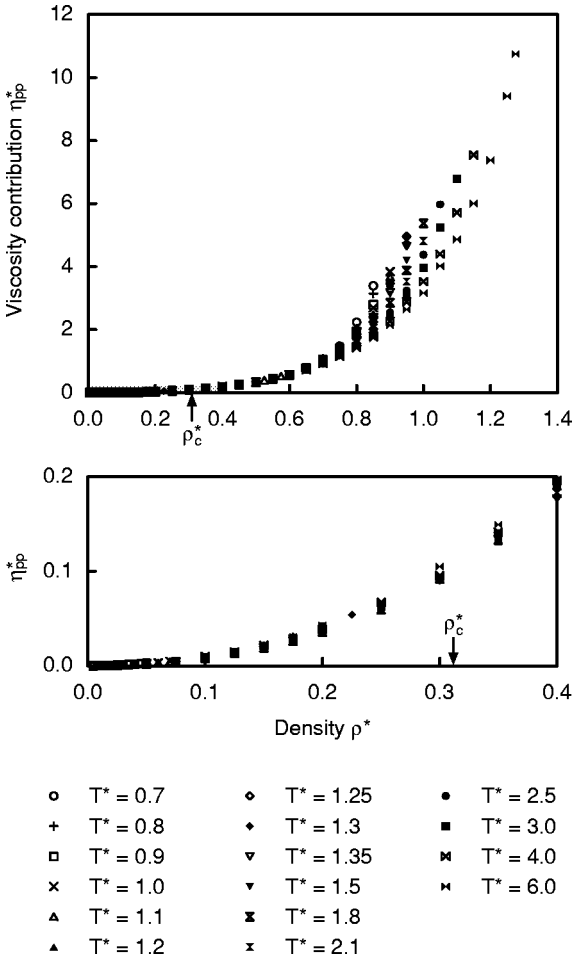

FIG. 11. The potential-potential viscosity contribution η^*_{pp} for all simulated isotherms as a function of density. The shaded area is enlarged in the bottom plot.

below $\rho^* \approx 0.2$ up to $T^* = 2.1$ and in the compressed liquid above $\rho^* \approx 0.8$ at increasing temperatures.

The isotherms of the kinetic-potential contribution are depicted in Fig. 10. Due to larger scatter of the data, the isotherms are not as clearly distinguishable as for the kinetic-kinetic contribution. This contribution vanishes in the limit of zero density, increases with density to a maximum at $\approx 2-2.5$ times the critical density and decreases at higher densities. The maximum of the isotherms is shifted to higher densities as the temperature increases. It occurs in that density range where the viscosity isotherms intersect.

Figure 11 shows the isotherms of the potential-potential viscosity contribution η^*_{pp}. The density dependence is more complex than that of η^*_{kk} and η^*_{kp}. This contribution depends only weakly on temperature up to densities of about $\rho^* = 0.7$. From this point, the isotherms split and diverge. The splitting occurs in the same density range where the η^*_{kp} isotherms exhibit their maxima and the viscosity isotherms intersect. In the high-density region, η^*_{pp} decreases with temperature.

Figure 12 displays the potential-potential viscosity contribution η^*_{pp} for selected isochors. Since the values of η^*_{pp} extend over several orders of magnitude, the isochors for liquid densities are displayed on a linear scale, and the gaseous isochors are given in semilogarithmic representation. The isochoric representation reveals that the temperature dependence of η^*_{pp} up to the point where the isotherms split is more complex than the isothermal representation, Fig. 11, indicates. Above the critical density, the isochors $\rho^* = 0.45$ and 0.6 are indeed almost constant in this representation. Increasing the resolution (not visible here) reveals that they increase slightly with temperature. In the gas region, the isochors decrease steeply at subcritical temperatures, but show little dependence on temperature at supercritical temperatures.

With the observed rather different and complex behavior of the three viscosity contributions, the viscosity surface in Figs. 7 and 8 can be understood much better. At high liquid densities, the potential-potential contribution η^*_{pp} dominates, while in the gas region the kinetic-kinetic contribution η^*_{kk} yields the largest contribution to the viscosity. The temperature dependence of the viscosity follows that of the dominating contribution. The minima on the viscosity isochors are caused by the superposition of the temperature dependences of η^*_{pp}, on one hand, and η^*_{kk} and of η^*_{kp}, on the other.

In Fig. 13, the results for the viscosity and its three contributions are depicted for the second simulation series at subcritical gaseous states. Due to the much longer production phases of 150 000 reduced time units, the data are far more accurate than the data at the same state points of the first series, whose simulations extended over only 6000 reduced time units. Besides this work, only Rowley and Painter[24] computed six viscosity data in this region. They are not shown in Fig. 13 because their uncertainty is much higher than the uncertainty of the present data. The present simulations were carried out in an attempt to determine the behavior of the viscosity in the gas region at low temperatures

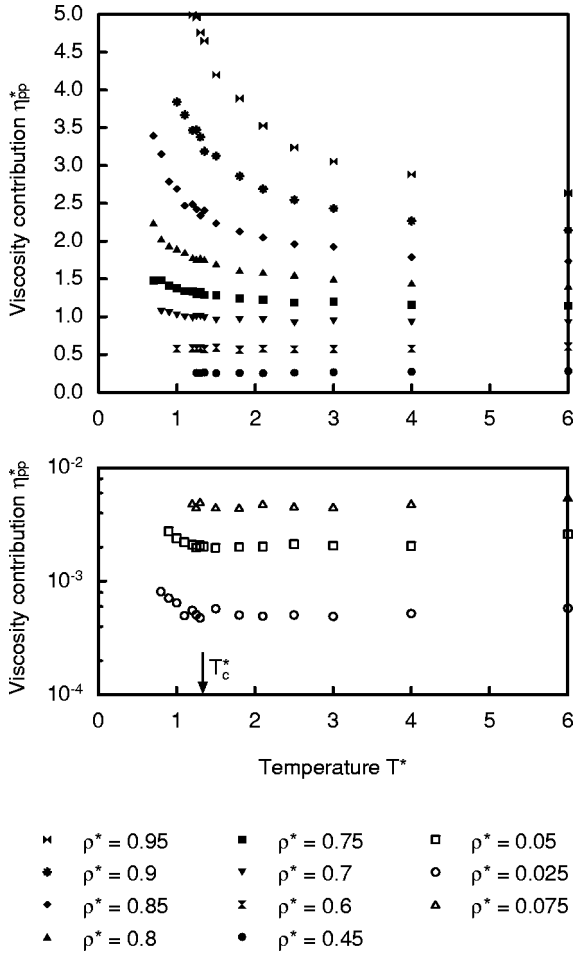

FIG. 12. The potential-potential viscosity contribution η^*_{pp} for selected isochors as a function of temperature.

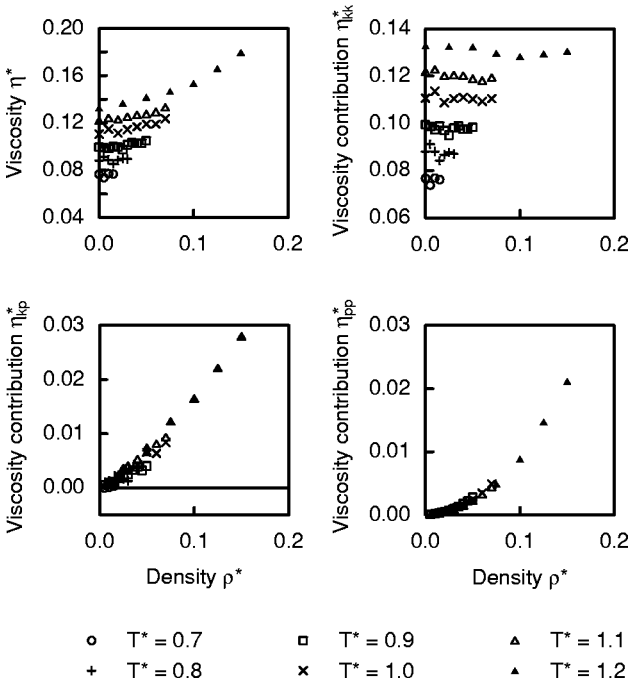

FIG. 13. The viscosity η^* and the viscosity contributions η^*_{kk}, η^*_{kp}, and η^*_{pp} for subcritical isotherms as a function of density. Symbols at zero density denote the Chapman-Enskog solution to the Boltzmann equation.

more accurately. Rainwater and Friend have shown that the initial slope of the viscosity isotherms of the Lennard-Jones model fluid becomes negative at reduced temperatures below about $T^*=1.0$. Measurements of the viscosity of real fluids have established that the decrease turns into an increase of the viscosity with density after a temperature-specific minimum is passed.[67] For instance, the viscosity correlation for propane by Vogel *et al.*[68] yields a minimum on the isotherm $T=280$ K between the densities $\rho=$ 0.11 to 0.14 mol dm^{-3}. With the reported scaling parameters $\sigma=0.497\,48$ nm and $\varepsilon/k=263.88$ K, these states correspond to the reduced density range between $\rho^*=0.008$ and 0.01 on the isotherm $T^*=0.942$ of the Lennard-Jones model fluid.

The viscosity on the two highest isotherms $T^*=1.1$ and 1.2 increases with density, while on the isotherms $T^*=0.9$ and 1.0 an increase occurs near the dew line. It cannot be discerned unambiguously whether or not the initial slope of these isotherms is negative and viscosity minima exist, because the scatter of the data is too high at the lowest densities. For the two lowest isotherms $T^*=0.7$ and 0.8, the density dependence cannot be assessed due to the scatter of the data. In spite of the extensive simulation lengths, the scatter of the data is still too high to determine the shape of the isotherms unambiguously. For a definitive determination of the initial slopes of the viscosity isotherms and their shape, substantially longer runs than those of the present simulations are required.

In Fig. 11, the isotherms of the potential-potential viscosity contribution are extremely flat at low densities. This raises the question whether the initial slope of the isotherms is zero or takes small nonzero values. Negative initial slopes are not possible as η^*_{pp} is zero at zero density and must always be positive at higher densities. At low densities, η^*_{pp} can be expressed by the series expansion

$$\eta^*_{pp}=B^*_{\eta_{pp}}(T^*)\rho^*+\cdots, \tag{11}$$

where the second potential-potential viscosity virial coefficient $B^*_{\eta_{pp}}$ is the initial slope at the temperature T^*. To determine the value of the initial slope, a method suggested by Prausnitz *et al.*[69] for the derivation of second virial coefficients of the pressure-density expansion from experimental pvT data is adopted. If the simulation data for η^*_{pp} are divided by density and the results are plotted versus density, $B^*_{\eta_{pp}}(T^*)$ is found by extrapolating the η^*_{pp}/ρ^* isotherm to zero density. This can be verified by

$$\lim_{\rho\to 0}\frac{\eta_{pp}}{\rho}=\frac{\text{“0”}}{\text{“0”}}=\lim_{\rho\to 0}\frac{\partial\eta_{pp}}{\partial\rho}, \tag{12}$$

in which the rule of de l'Hospital has been applied to evaluate the limit. This method can also be used to determine the initial slope of the η^*_{kp} isotherms, $B^*_{\eta_{kp}}(T^*)$, since η^*_{kp} becomes zero in the zero-density limit.

Figure 14 depicts the calculated ratios η^*_{kp}/ρ^* and η^*_{pp}/ρ^* for the six subcritical isotherms of the second simulation series. The data for the kinetic-potential viscosity contribution scatter, but it is evident that $B^*_{\eta_{kp}}$ increases with

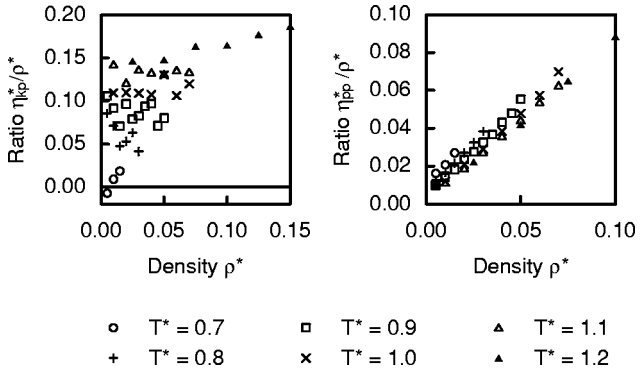

FIG. 14. The ratios η^*_{kp}/ρ^* and η^*_{pp}/ρ^* at gaseous states on subcritical isotherms as a function of density.

temperature, as could be expected from the discussion of Fig. 10. Moreover, the extrapolation of the η^*_{pp}/ρ^* isotherms shows that the second potential-potential viscosity virial coefficient $B^*_{\eta_{pp}}$ is nonzero and that it decreases with temperature between $T^*=0.7$ and 1.2.

Since the mean free path between collisions might become as large as the length of the simulation cube at low densities, one might suspect that the simulation data are subject to systematic errors. To check the data for this effect, one simulation at the state point ($T^*=0.9$, $\rho^*=0.005$) was repeated with 256 instead of 1372 particles, but otherwise unchanged simulation parameters. Since the simulation cube is smaller with fewer particles, a systematic effect is expected to be stronger. However, the result for η^*_{pp} agreed with that obtained with 1372 particles within 0.1%. Therefore, the size of the simulation cube appears to have no influence on the present investigation. Probably, the application of periodic boundary conditions reduces the influence of the system size.

IX. SHEAR-STRESS CORRELATION FUNCTIONS

When using the Green-Kubo integral formulas instead of the Einstein relations, Eqs. (7)–(9), the viscosity contributions,

$$\eta_{kk}=\frac{V}{kT}\int_0^\infty \langle \tau_{xy,k}(0)\tau_{xy,k}(t)\rangle dt, \tag{13}$$

$$\eta_{kp}=\frac{V}{kT}\int_0^\infty \langle \tau_{xy,p}(0)\tau_{xy,k}(t)+\tau_{xy,k}(0)\tau_{xy,p}(t)\rangle dt, \tag{14}$$

$$\eta_{pp}=\frac{V}{kT}\int_0^\infty \langle \tau_{xy,p}(0)\tau_{xy,p}(t)\rangle dt, \tag{15}$$

are related to the integrals of the shear-stress correlation functions. Therefore, their temperature and density dependence can be interpreted by the decay behavior of these correlation functions. For this purpose, the total correlation functions are separated into the three contributions $\langle \tau^*_k(0)\tau^*_k(t)\rangle$, $\langle \tau^*_p(0)\tau^*_k(t)+\tau^*_k(0)\tau^*_p(t)\rangle$, and $\langle \tau^*_p(0)\tau^*_p(t)\rangle$, which correspond to the viscosity contributions η^*_{kk}, η^*_{kp}, and η^*_{pp}. The discussion focuses on selected state points that are representative examples for the behavior of the shear-stress correlation function in the fluid region. In some instances, time derivatives, time integrals, or double logarithmic representations of the correlation functions are given to illustrate their decay behavior. The representation is chosen so that the effects are optimally visible. In all figures of this section, normalized shear-stress correlation functions are shown. The normalization factor is omitted to keep the notation as simple as possible. Kinetic-kinetic and potential-potential shear-stress correlation functions are normalized by their initial values, while kinetic-potential correlation functions are normalized by their maximum value.

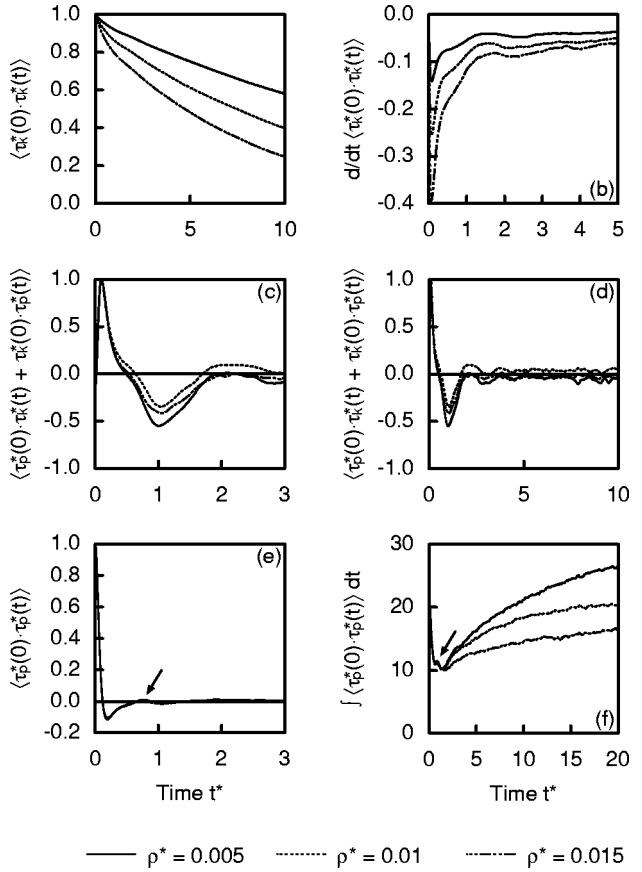

FIG. 15. Normalized shear-stress correlation functions for selected densities on the lowest simulated isotherm $T^*=0.7$ close to the triple point temperature. (a) Short-time behavior of kinetic-kinetic contribution; (b) time derivative of kinetic-kinetic contribution; (c) short-time behavior of kinetic-potential contribution; (d) long-time behavior of kinetic-potential contribution; (e) potential-potential contribution; (f) time integral function of potential-potential contribution. Note the different abscissa scales in the subfigures. The arrows point to special features of the correlation functions addressed in the text.

Figures 15 and 16 show the three contributions to the shear-stress correlation function at low densities in the gas region on the isotherm $T^*=0.7$ and the isochor $\rho^*=0.025$. The kinetic-kinetic contribution closely resembles the behavior of the velocity autocorrelation function in this state region.[10,54] At low temperatures, the decay of the kinetic-kinetic correlation functions is superimposed by small oscillations, which decay after a few cycles. The oscillations are clearly evident in the time derivatives of the correlation functions. The strongest effect is observed for the temperature $T^*=0.7$ close to the triple-point temperature. The magnitude of the oscillations increases with density, while the overall decay of the correlation function becomes faster. Along the

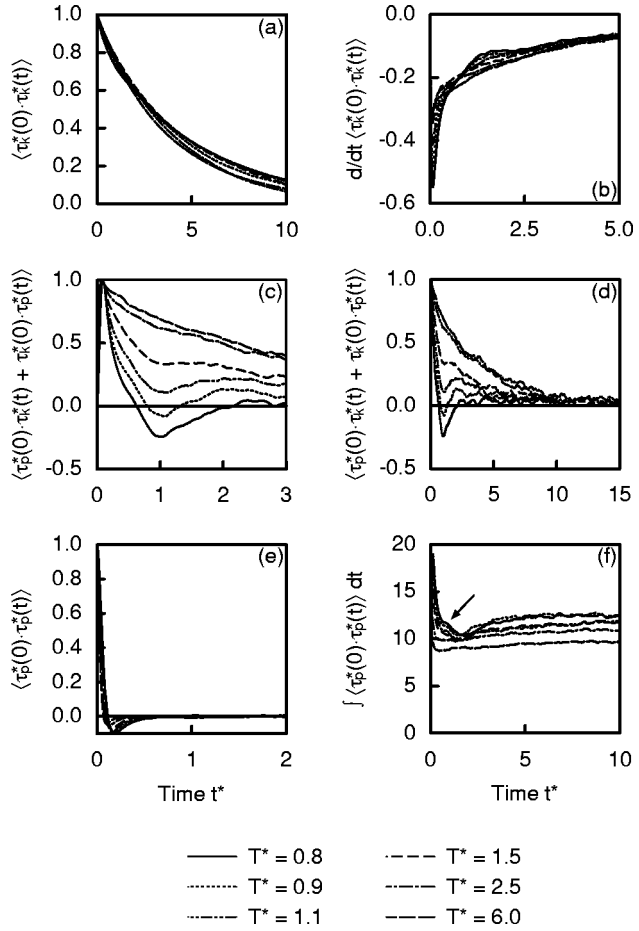

FIG. 16. Normalized shear-stress correlation functions for selected temperatures on the isochor $\rho^*=0.025$. (a) Short-time behavior of kinetic-kinetic contribution; (b) time derivative of kinetic-kinetic contribution; (c) short-time behavior of kinetic-potential contribution; (d) long-time behavior of kinetic-potential contribution; (e) potential-potential contribution; (f) time integral function of potential-potential contribution. Note the different abscissa scales in the subfigures. The arrow points to special features of the correlation functions addressed in the text.

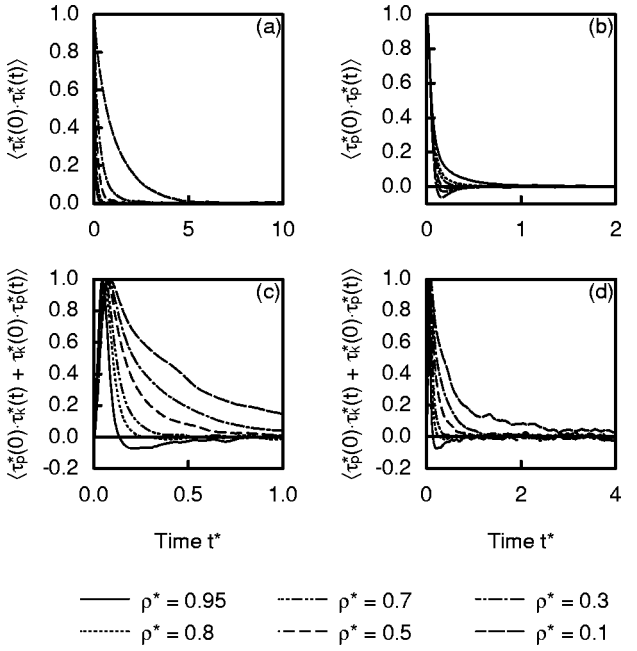

FIG. 17. Normalized shear-stress correlation functions for selected densities on the isotherm $T^*=1.35$. (a) Kinetic-kinetic contribution; (b) potential-potential contribution; (c) short-time behavior of kinetic-potential contribution; (d) long-time behavior of kinetic-potential contribution. Note the different abscissa scales in the subfigures.

isochor $\rho^*=0.025$, the oscillations become smaller with increasing temperature and vanish for the highest temperatures displayed in Fig. 16. Moreover, the kinetic-kinetic correlation functions decay more rapidly with increasing temperature. The similarities between kinetic-kinetic shear-stress correlation functions and velocity autocorrelation functions are not surprising since both functions measure correlations between particle velocities.

The cross contributions show a completely different behavior. At low temperatures, they start from zero, exhibit maxima, decrease to negative values, reach a minimum and increase to a second maximum before approaching the time axis. This complex behavior at short times is superimposed by small oscillations. Details of the long-time behavior cannot be assessed since it is hidden in stochastic noise. With increasing temperature, the minimum as well as the superimposed oscillations vanish, and the correlation function decreases monotonically from the first maximum to zero.

On the isotherm $T^*=0.7$, the potential-potential shear-stress correlation function appears to be almost independent of density. It decreases rapidly to negative values, reaches a minimum, then increases and oscillates several times before decaying monotonically to the time axis from above. This short-time behavior is similar to the oscillations observed in the short-time behavior of the kinetic-kinetic and kinetic-potential contributions. The corresponding time integrals reveal that the short-time behavior is indeed density-independent on this isotherm. However, the long-time behavior depends strongly on density and yields a significant contribution to η^*_{pp}. With increasing temperature, the first minimum on the isochor $\rho^*=0.025$ is lifted and shifted to earlier times. Furthermore, the contribution of the long-time decay to the integral of the potential-potential shear-stress correlation function decreases at high temperatures.

Oscillations in the potential-potential contribution to shear-stress correlation functions were also reported by Michels and Trappeniers[70] for square-well model fluids and attributed to the formation of bound states. The same effect is observed for the velocity autocorrelation functions of the Lennard-Jones model fluid at low densities.[10] The interpretation of this behavior by the formation of bound states is easier for the velocity autocorrelation function[71] because it involves only correlations between single particles and will therefore be given in the second paper of this series,[54] where the results for self-diffusion are discussed. The results for the shear-stress correlation functions provide further evidence for the existence of bound states at low temperatures.

Figure 17 shows the influence of density on the three contributions to the shear-stress autocorrelation function along the supercritical isotherm $T^*=1.35$ close to the critical temperature. The shape of the kinetic-kinetic shear-stress correlation functions is similar at all densities, with the decay becoming slower at low densities. At high densities, the

kinetic-kinetic correlation function does not show the negative regime at intermediate times found for the velocity autocorrelation functions in this state region.[10,54]

The decrease of the η_{kp}^* isotherms at high densities can be explained by the decay behavior of the kinetic-potential shear-stress correlation functions. All cross correlation functions have a maximum at short times. At low densities, the correlation functions decrease monotonically towards zero from this maximum. At high densities, however, the maximum is followed by a steep decrease to negative values and a pronounced negative region. This yields a significant negative contribution to the value of η_{kp}^*, causing the isotherm to decrease at high densities.

The decay of the potential-potential shear-stress correlation function also changes along the isotherm. With increasing density, the characteristic minimum observed at low densities vanishes, and the correlation functions decay monotonically. At the highest density, $\rho^*=0.95$, the rapid decay at short times is followed by a pronounced slow decay up to at least one reduced time unit. The slow decay occurs in that time regime where the negative regions for the cross correlation function and velocity autocorrelation function are found.[10] This observation indicates a close relation between the relevant mass and momentum transport mechanisms on the molecular scale.

Stassen and Steele[27,28] examined the decay of the contributions to the shear-stress correlation functions at the subcritical isotherm $T^*=1.26$ at five state points between $\rho^*=0.211$ and $\rho^*=0.844$. Moreover, they calculated the two-, three- and four-body contributions to the potential-potential shear-stress correlation functions as described in Sec. II. At low densities, the three- and four-body contributions are very small and cancel each other so that the potential-potential shear-stress correlation function is dominated by the two-body contribution. At high densities, the short-time behavior of all contributions was found to be relatively complex. Both, the three- and four-body contributions yield larger contributions to the potential-potential shear-stress correlation function. Surprisingly, the behavior of the two-body contribution found at low densities is almost unchanged at high densities, with the minimum being moved to positive values. The monotonic decay of the potential-potential shear-stress correlation function at high densities results from the superposition of the three contributions.

The influence of temperature on the decay of shear-stress correlation functions is shown in Figs. 18 and 19 for the isochors $\rho^*=0.3$ and $\rho^*=0.85$. On the isochor $\rho^*=0.3$, the characteristic decay behavior depends only weakly on temperature for all three viscosity contributions. Due to increased scattering, the decay of the kinetic-kinetic contribution becomes faster at high temperatures. This effect lowers the time integral of the normalized correlation function. The potential-potential contribution shows the minimum typical for low densities at short times at all displayed temperatures. At high temperatures, the minimum is lifted and shifted to earlier times as already observed for the isochor $\rho^*=0.025$. At this density, the constant plateau values of the integrated time-correlation functions are reached within a few reduced time units.

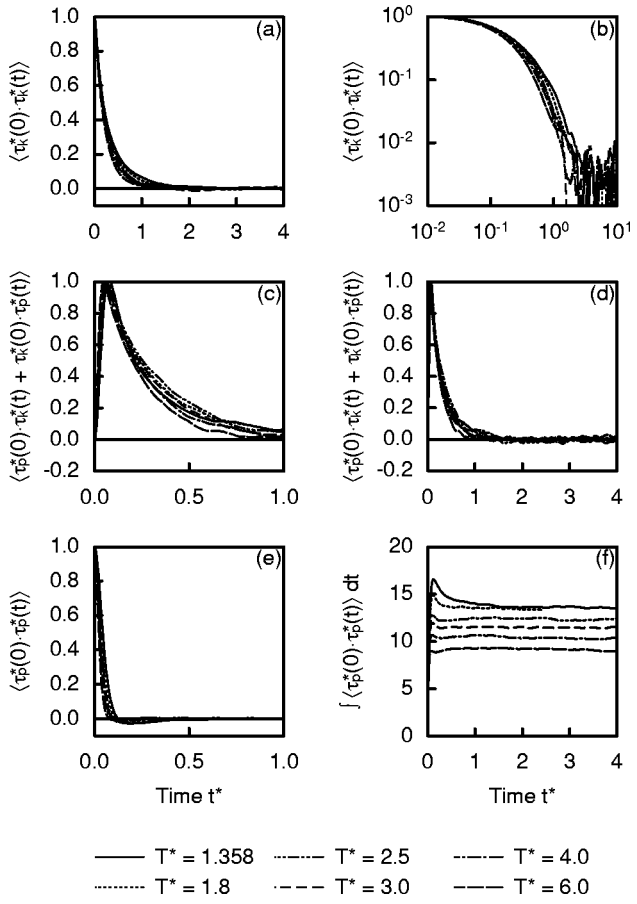

FIG. 18. Normalized shear-stress correlation functions for selected temperatures on the isochor $\rho^*=0.3$ close to the critical density. (a) Kinetic-kinetic contribution; (b) kinetic-kinetic contribution in double logarithmic representation; (c) short-time behavior of kinetic-potential contribution; (d) long-time behavior of kinetic-potential contribution; (e) potential-potential contribution; (f) time integral function of potential-potential contribution. Note the different abscissa scales in the subfigures.

Along the isochor $\rho^*=0.85$, the influence of temperature on the kinetic-kinetic and cross contribution is similar. At all temperatures, the cross contribution shows the negative region at intermediate times that causes the decay of the isotherms at high densities. The decay behavior of the potential-potential contribution depends strongly on temperature. At low temperatures, a pronounced slow decay at intermediate times is observed. This effect becomes smaller with increasing temperature. The slow decay occurs in the same time regime where the cross correlation function is negative.

As a final point, the question is addressed whether the contributions to the shear-stress correlation functions show long-time tails, e.g., their decay at long times follows a power law. Theoretical calculations of the long-time behavior by mode-coupling approaches support the existence of long-time tails of the form $\sim t^{-3/2}$ for all three contributions.[72] This issue has previously been investigated by molecular-dynamics simulations.[34,52] However, due to the large demand for computational resources for an accurate determination of the correlation functions at long times the problem has not yet been solved.

The kinetic-kinetic contributions to the correlation functions at both densities, $\rho^*=0.3$ and $\rho^*=0.85$, and the

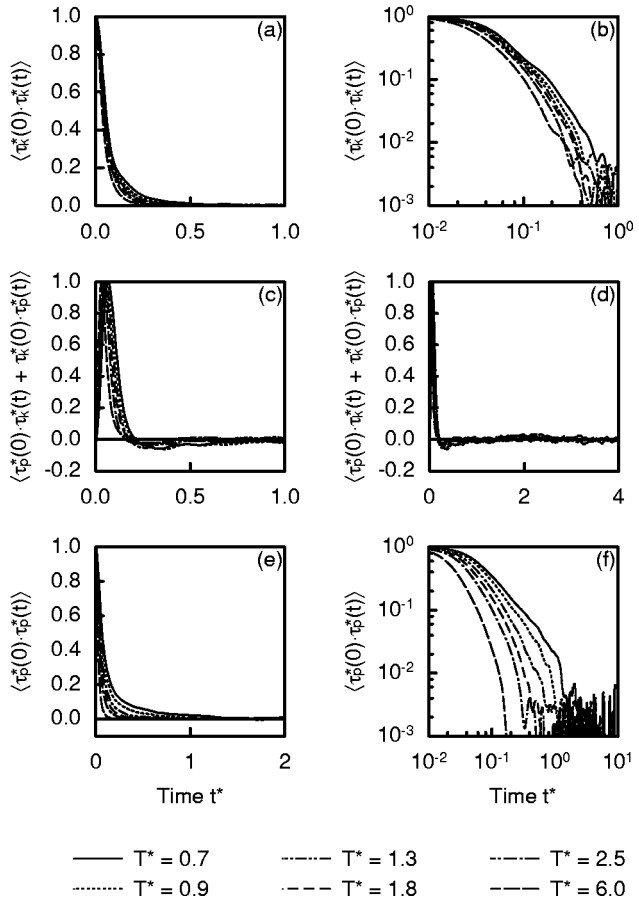

FIG. 19. Normalized shear-stress correlation functions for selected temperatures on the liquid isochor $\rho^*=0.85$. (a) Kinetic-kinetic contribution; (b) kinetic-kinetic contribution in double logarithmic representation; (c) short-time behavior of kinetic-potential contribution; (d) long-time behavior of kinetic-potential contribution; (e) potential-potential contribution; (f) potential-potential contribution in double logarithmic representation. Note the different abscissa scales in the subfigures.

potential-potential contributions at $\rho^*=0.85$ are depicted in Figs. 18 and 19 in double logarithmic representation. In this representation, the long-time tails should appear as straight lines with the slope -1.5. Since long-time tails with the exponent -1.5 were found for the velocity autocorrelation functions at high densities and temperatures,[10,54] it is expected that the predicted behavior is preferably observable in this state region.

On the isochor $\rho^*=0.85$, linear decay appears to exist for the kinetic-kinetic contribution at the lowest displayed temperature $T^*=0.7$ between $t^*=0.2$ and 0.5. The exponent from a linear least-squares fit is ≈ -2.2. At the higher temperatures $T^*=0.9$, 1.3, and 1.8, the ''linear'' decay starts slightly earlier with increasing temperature. At the two highest temperatures, the decay is certainly faster than linear. For the potential-potential contribution, the expected straight lines with the slope -1.5 appear to exist for the two lowest displayed temperatures $T^*=0.7$ and 0.9 at about one reduced time unit. However, from the results for the velocity autocorrelation functions[10,54] the linear decay is expected to start later. At higher temperatures, the decay is faster, becoming exponential at the highest temperatures. On the isochor $\rho^*=0.3$, the kinetic-kinetic contribution does not show the expected linear decay.

The time periods in which linear decay is observed are relatively short, so that the existence of the long-time tails in shear-stress correlation functions cannot be unambiguously established with the present simulation results. The analysis of the shear-stress correlation functions at longer times is hindered by the high noise level. Much longer simulations than the present ones are required to precisely resolve the long-time behavior of the shear-stress correlation functions.

X. CONCLUSIONS

The viscosity of the Lennard-Jones model fluid was determined by equilibrium molecular dynamics simulations over a broad range of state points in the fluid region of the phase diagram using the Einstein relation method. By use of more particles, larger cutoff radii, and much longer simulation runs than considered before in conventional simulation work, the present simulation data for the viscosity are significantly more accurate than those of previous studies. The uncertainty of the data is estimated to be $\pm 3\%$ at liquid densities, increasing up to $\pm 10\%$ at low-density gaseous states. The high accuracy of the present data is demonstrated by comparisons with literature data. With the accurate and comprehensive data, coherent insights into the nature of the viscosity from previously little-explored view angles are possible. The kinetic-kinetic, kinetic-potential and potential-potential viscosity contributions are resolved over the whole range of fluid states, and their characteristic dependence on temperature and density is described. Moreover, analysis of the shear-stress correlation functions reveals aspects of the transport mechanisms on the molecular scale.

ACKNOWLEDGMENTS

K.M. acknowledges an appointment as a guest researcher at the Physical and Chemical Properties Division of the National Institute of Standards and Technology in Boulder during the summer of 1999, where parts of this research were carried out. Computational resources for this work were provided by the Regional Computing Center for Lower Saxony at the University of Hannover (RRZN), the Konrad-Zuse-Zentrum for Information Technology in Berlin and the NIST Information Technology Laboratory in Gaithersburg, Maryland. We acknowledge the assistance of Dr. Simone Knief and Jürgen Fischer (RRZN) with the parallelization of the software and the assistance of Denis Lehane at NIST.

[1] J. O. Hirschfelder, C. F. Curtiss, and R. B. Bird, *Molecular Theory of Gases and Liquids* (Wiley, New York, 1954).
[2] R. Zwanzig, Annu. Rev. Phys. Chem. **16**, 67 (1965).
[3] J. A. McLennan and R. J. Swenson, J. Math. Phys. **4**, 1527 (1963).
[4] S. Alavi and R. F. Snider, J. Chem. Phys. **109**, 3452 (1998).
[5] R. F. Snider and S. Alavi, J. Chem. Phys. **111**, 6909 (1999); S. Alavi and R. F. Snider, *ibid.* **111**, 6922 (1999).
[6] D. K. Hoffman and C. F. Curtiss, Phys. Fluids **7**, 1887 (1964); **8**, 667 (1965); **8**, 890 (1965); R. F. Snider and C. F. Curtiss, *ibid.* **1**, 122 (1958).
[7] S. K. Nath, B. J. Banaszak, and J. J. de Pablo, J. Chem. Phys. **114**, 3612 (2001).
[8] http://ts.nist.gov/ts/htdocs/230/232/232.htm
[9] K. Meier, A. Laesecke, and S. Kabelac, Int. J. Thermophys. **22**, 161 (2001).

[10] K. Meier, *Computer Simulation and Interpretation of the Transport Coefficients of the Lennard-Jones Model Fluid* (Shaker, Aachen, 2002).
[11] D. J. Evans and G. P. Morriss, *Statistical Mechanics of Nonequilibrium Liquids* (Academic, London, 1990).
[12] W. G. Hoover, *Computational Statistical Mechanics* (Elsevier, Amsterdam, 1991).
[13] G. Arya, E. J. Maginn, and H.-C. Chang, J. Chem. Phys. **113**, 2079 (2000).
[14] F. Müller-Plathe, Phys. Rev. E **59**, 4894 (1999).
[15] S. Y. Liem, D. Brown, and J. H. R. Clarke, Phys. Rev. A **45**, 3706 (1992).
[16] K. P. Travis, D. J. Searles, and D. J. Evans, Mol. Phys. **95**, 195 (1998).
[17] J. Petravic and D. J. Evans, Mol. Phys. **95**, 219 (1998).
[18] M. S. Green, J. Chem. Phys. **20**, 1281 (1952); **22**, 398 (1954).
[19] R. Kubo, J. Phys. Soc. Jpn. **12**, 570 (1957); R. Kubo, M. Yokota, and S. Nakajima, *ibid.* **12**, 1203 (1957).
[20] E. Helfand, Phys. Rev. **119**, 1 (1960).
[21] J. M. Haile, *Molecular Dynamics Simulation—Elementary Methods* (Wiley, New York, 1992).
[22] J. J. Erpenbeck, Phys. Rev. E **51**, 4296 (1995).
[23] M. Schoen, Dr. rer. nat.-Thesis, Abteilung für Chemie, Ruhr-Universität Bochum, 1986.
[24] R. L. Rowley and M. M. Painter, Int. J. Thermophys. **18**, 1109 (1997).
[25] M. P. Allen and D. J. Tildesley, *Computer Simulation of Liquids* (Clarendon, Oxford, 1987).
[26] S. Sharma, Ph.D. thesis, Chemical Engineering Department, University of Bradford, 1994.
[27] H. Stassen and W. A. Steele, J. Chem. Phys. **102**, 932 (1995).
[28] H. Stassen and W. A. Steele, J. Chem. Phys. **102**, 8533 (1995).
[29] R. Lustig, J. Chem. Phys. **100**, 3048 (1994).
[30] J. R. Ray and H. Zhang, Phys. Rev. E **59**, 4781 (1999).
[31] R. Friedberg and J. E. Cameron, J. Chem. Phys. **52**, 6049 (1970).
[32] R. Agrawal and D. A. Kofke, Mol. Phys. **85**, 43 (1995).
[33] D. Levesque, L. Verlet, and J. Kürkijarvi, Phys. Rev. A **7**, 1690 (1973).
[34] J. J. Erpenbeck, Phys. Rev. A **38**, 6255 (1988).
[35] J. J. Erpenbeck, Phys. Rev. A **35**, 218 (1987).
[36] D. J. Evans, G. P. Morriss, and L. M. Hood, Mol. Phys. **68**, 637 (1989).
[37] S. Sharma and L. V. Woodcock, J. Chem. Soc., Faraday Trans. **87**, 2023 (1991).
[38] D. M. Heyes, J. Chem. Phys. **85**, 997 (1986).
[39] W. T. Ashurst and W. G. Hoover, Phys. Rev. A **11**, 658 (1975).
[40] D. J. Evans, Phys. Rev. A **23**, 1988 (1981).
[41] D. M. Heyes, J. J. Kim, C. J. Montrose, and T. A. Litovitz, J. Chem. Phys. **73**, 3987 (1980).
[42] D. M. Heyes, Phys. Rev. B **37**, 5677 (1988).
[43] D. M. Heyes and J. G. Powles, Mol. Phys. **71**, 781 (1990).
[44] D. M. Heyes, J. Chem. Soc., Faraday Trans. 2 **79**, 1741 (1983).
[45] D. M. Heyes, Can. J. Phys. **64**, 773 (1986).
[46] W. G. Hoover, D. J. Evans, R. B. Hickman, A. J. C. Ladd, W. T. Ashurst, and B. Moran, Phys. Rev. A **22**, 1690 (1980).
[47] D. Levesque and L. Verlet, Mol. Phys. **61**, 143 (1987).
[48] E. L. Pollock, Simulation data reported by Hoover *et al.* in Ref. 46.
[49] M. Schoen and C. Hoheisel, Mol. Phys. **56**, 653 (1985).
[50] K. Singer, J. V. L. Singer, and D. Fincham, Mol. Phys. **40**, 515 (1980).
[51] C. Trozzi and G. Cicotti, Phys. Rev. A **29**, 916 (1984).
[52] M. Ferrario, G. Cicotti, B. L. Holian, and J. P. Ryckaert, Phys. Rev. A **44**, 6936 (1991).
[53] M. Mecke, A. Müller, J. Winkelmann, J. Vrabec, J. Fischer, R. Span, and W. Wagner, Int. J. Thermophys. **17**, 391 (1996).
[54] K. Meier, A. Laesecke, and S. Kabelac, J. Chem. Phys. (to be published).
[55] K. Meier, A. Laesecke, and S. Kabelac (unpublished).
[56] K. Meier, A. Laesecke, and S. Kabelac, (unpublished).
[57] See EPAPS Document No. E-JCPSA6-121-505430 for text files and color figures. A direct link to this document may be found in the online article's HTML reference section. The document may also be reached via the EPAPS homepage (http://www.aip.org/pubservs/epaps.html) or from ftp.aip.org in the directory /epaps/. See the EPAPS homepage for more information.
[58] ftp://FTP.Boulder.NIST.Gov/pub/fluids/Lennard-Jones
[59] P. Borgelt, C. Hoheisel, and G. Stell, Phys. Rev. A **42**, 789 (1990).
[60] M. Canales and J. A. Padró, Phys. Rev. E **60**, 551 (1999).
[61] B. L. Holian and D. J. Evans, J. Chem. Phys. **78**, 5147 (1983).
[62] D. M. Heyes, J. Chem. Soc., Faraday Trans. 2 **83**, 1985 (1987).
[63] K. D. Hammonds and D. M. Heyes, J. Chem. Soc., Faraday Trans. 2 **84**, 705 (1988).
[64] D. M. Heyes, J. G. Powles, and J. C. Gil Montero, Mol. Phys. **78**, 229 (1993).
[65] J. P. J. Michels and N. J. Trappeniers, Physica A **133**, 281 (1985).
[66] H. J. M. Hanley, R. D. McCarty, and W. M. Haynes, J. Phys. Chem. Ref. Data **3**, 979 (1974).
[67] J. C. Rainwater, J. Chem. Phys. **81**, 495 (1984); D. G. Friend and J. C. Rainwater, Chem. Phys. Lett. **107**, 590 (1984); J. C. Rainwater and D. G. Friend, Phys. Rev. A **36**, 4062 (1987); E. Bich and E. Vogel, in *Initial Density Dependence*, Transport properties of fluids: their correlation, prediction and estimation, edited by J. Millat, J. H. Dymond, and C. A. Nieto de Castro (Cambridge University, Cambridge, 1996), pp. 72–82.
[68] E. Vogel, C. Küchenmeister, E. Bich, and A. Laesecke, J. Phys. Chem. Ref. Data **27**, 947 (1998).
[69] J. M. Prausnitz, R. N. Lichtenthaler, and E. G. de Azevedo, *Molecular Thermodynamics of Fluid-Phase Equilibria*, 2nd edition (Prentice-Hall, Englewood Cliffs, NJ, 1986).
[70] J. P. J. Michels and N. J. Trappeniers, Physica A **107**, 299 (1981).
[71] J. P. J. Michels and N. J. Trappeniers, Chem. Phys. Lett. **33**, 195 (1975).
[72] M. H. Ernst, E. H. Hauge, and J. M. J. van Leeuwen, Phys. Rev. A **4**, 2055 (1971); J. Stat. Phys. **15**, 7 (1976); **15**, 23 (1976).